A Novel Supercritical CO_2 Foam System Stabilized With a Mixture of Zwitterionic Surfactant and Silica Nanoparticles for Enhanced Oil Recovery

Weitao Li[1]*, Falin Wei[1], Chunming Xiong[1], Jian Ouyang[1], Liming Shao[1], Mingli Dai[1], Pingde Liu[1] and Dongxing Du[2]

[1] Department of Oilfield Chemicals, Research Institute of Petroleum Exploration & Development, PetroChina, Beijing, China, [2] College of Electromechanical Engineering, Qingdao University of Science and Technology, Qingdao, China

In order to improve the CO_2 foam stability at high temperature and salinity, hydrophilic silica nanoparticles (NPs) were added into a dilute zwitterionic surfactant solution to stabilize supercritical CO_2 (SC-CO_2) foam. In the present paper, the foaming capacity and stability of SC-CO_2 foam were investigated as a function of NP concentration at elevated temperatures and pressures. It was observed that the drainage rate of SC-CO_2 foam was initially fast and then became slower with NPs adsorption at the gas-liquid interface. The improved foam stability at high temperature was attributed to the enhanced disjoining pressure with addition of NPs. Furthermore, an obvious increase in the foam stability was noticed with the increasing salinity due to the screening of NP charges at the interface. The rheological characteristics including apparent viscosity and surface elasticity, resistance factor, and microstructures of SC-CO_2 foam were also analyzed at high temperature and pressure. With addition of 0.7% NPs, SC-CO_2 foam was stabilized with apparent viscosity increased up to 80 mPa·s and resistance factor up to 200. Based on the stochastic bubble population (SBP) model, the resistance factor of SC-CO_2 foam was simulated by considering the foam generation rate and maximum bubble density. The microstructural characteristics of SC-CO_2 foam were detected by optical microscopy. It was found that the effluent bubble size ranged between 20 and 30 μm and the coalescence rate of SC-CO_2 foam became slow with the increasing NP concentration. Oscillation measurements revealed that the NPs enhanced surface elasticity between CO_2 and foam agents for resisting external disturbances, thus resulting in enhanced film stability and excellent rheological properties.

Keywords: supercritical CO_2 foam, silica nanoparticles, foam stability, rheological properties, mobility control

INTRODUCTION

CO_2 flooding is a widely applied enhanced oil recovery (EOR) method due to its easy miscibility with crude oil, thereby resulting in an expanded oil volume and a decrease in oil viscosity (Sanders et al., 2012; Mukherjee et al., 2014). However, the occurrence of an early CO_2 breakthrough leads to a poor sweep efficiency and high operating cost due to gravity override, viscous fingering, and

formation heterogeneity (Chang and Grigg, 1999; Farajzadeh et al., 2012; Ayesh et al., 2017). CO_2 foam or chemical gels are the most common agents to improve the macroscopic sweep efficiency by controlling the mobility of CO_2 in high-permeability zones. Polymer gels are often used to plug thief zones by diverting CO_2 to other zones (Chang and Grigg, 1999; Zhang et al., 2019); however, they usually exist near the wellbore and manifest a limited effect on deep formation control (Zhang and Seright, 2007). CO_2 foam, which is a dispersion of discontinuous CO_2 in the liquid phase, can overcome the aforesaid drawbacks and is regarded as one of the effective mobility control agents for CO_2 flooding. CO_2 foam is extensively applied to improve the sweep efficiency of heterogeneous reservoirs by reducing gas relative permeability and increasing gas viscosity (Lotfollahi et al., 2016). When the reservoir temperature and pressure exceed the critical point of CO_2 (31.1°C and 7.37 MPa, respectively), gaseous CO_2 is usually transformed into a dense, liquid-like fluid (supercritical CO_2) (Chang and Grigg, 1999). The viscosity of supercritical CO_2 generally remains very low, whereas its density (0.5–0.9 g/cm^3) is found to be significantly higher than that of gaseous CO_2. Therefore, the physical properties of supercritical CO_2 and gaseous CO_2 are completely different under ambient conditions. Moreover, when supercritical CO_2 is dispersed into a surfactant solution, CO_2 foam manifests much better solubility, pH, texture, and mobility as compared to gaseous CO_2 foam.

However, the stability of CO_2 foam generally deteriorates under harsh reservoir conditions (high temperature and salinity) (Chen et al., 2015; Chang et al., 2018). Foam stability can be considered as the stability of a bubble film and is determined by numerous factors including bulk viscosity, surface viscoelasticity, Marangoni effect, and disjoining pressure (Tamura et al., 1997). In addition, film stability is also affected by the temperature, salinity, pressure, and pore structure of a porous media. In order to improve foam stability, different foaming agents including surfactants (Basheva et al., 1999; Dhanuka et al., 2006), nanoparticles (NPs) (Basheva et al., 1999; Stephanie et al., 2008; Worthen et al., 2014), and polymers (Basheva et al., 1999; Petkova et al., 2012; Kalyanaraman et al., 2016) have been incorporated into CO_2 foam. The apparent viscosity of SC-CO_2 foam stabilized with surfactants and polymers is significantly higher (by several orders of magnitude) than that of a pure gaseous foam (Da et al., 2018). However, the strength or solubility of surfactants and polymers starts to degrade under high temperatures and salinity, thereby resulting in poor foam stability. NPs are the most effective agent to stabilize CO_2 foam due to their high chemical stability at high temperature and salinity (Alzobaidi et al., 2017). Silica nanoparticles can form compact coherent particle shells at the gas-liquid interface, thus resulting in improved foam stability by resisting film deformation (Horozov, 2008). The effectiveness of solid particles depends on their sizes, shapes, concentrations, and wettability. When wetted ($\theta = 0°$) or dewetted ($\theta = 180°$) solid particles remain dispersed in the liquid phase or the gas phase, no stable liquid film is generally formed. When the contact angle (θ) ranges between 0° and 180°, solid particles start to agglomerate in liquid films. The aqueous and gaseous phases are the preferred accumulation sites for hydrophilic ($0° < \theta < 90°$) and

hydrophobic particles ($90° < \theta < 180°$), respectively (Aveyard and Clint, 1995).

It is found that hexadecyl hydroxypropyl sulfobetaine (HHSB; a zwitterionic surfactant) can generate SC-CO_2 foam under high temperature (up to 90°C) and salinity (25×10^4 mg/L). However, as temperature was higher than 90°C, the stability of SC-CO_2 foam declined sharply. In the present work, in order to improve the stability of SC-CO_2 foam at high temperatures, hydrophilic silica NPs were added to a dilute HHSB solution. Furthermore, previous researches have mainly focused on the capacity of NPs-stabilized CO_2 foam at atmospheric pressure and room temperature. Thus, we presented a detailed investigation on effect of NPs on SC-CO_2 foam. The stability, rheological characteristics and stabilization mechanism of SC-CO_2 foam were explored with an increase in the NP concentration.

MATERIALS AND METHODS

Materials

HHSB ($C_{16}H_{33}N(CH_3)_2CH_2CH(OH)CH_2SO_3$) was procured from Shanghai Nuosong Chemical Co. Ltd., China. Hydrophilic silica nanoparticles (average size of 65 nm) were purchased as a 30% concentration aqueous solution from Sigma-Aldrich. Sodium chloride and calcium chloride were obtained from Beijing Chemical Works, China. Four types of the formation brine (the amounts of dissolved solid were 2×10^4 mg/L, 5×10^4 mg/L, 7×10^4 mg/L, and 10×10^4 mg/L) were prepared by adding NaCl and CaCl$_2$ (in a ratio of 9:1) into deionized (DI) water.

Evaluation of SC-CO_2 Foaming Capacity and Stability

The schematic diagram of the apparatus used for assessing the capacity and stability of SC-CO_2 foam at high temperatures and pressures is displayed in **Figure 1**. CO_2 in the gas tank was first pressurized to the desired pressure and then put into the gas container in the oven. After CO_2 was heated to the desired temperature, supercritical CO_2 was injected into the high-pressure view chamber. The HHSB/NPs solution (100 mL) was then pumped into the chamber. Finally, when the desired pressure and temperature were attained in the chamber, the mixture was sheared at 2,000 rpm for 5 min. The maximum foaming volume was recorded to assess the foaming ability of foaming agents. The liquid volume separated from the foam was recorded as a function of time. In order to evaluate the foam stability, the half-life of the foam was defined as the time when half of the liquid was drained from the foam.

Rheological Measurements

The apparent viscosity of SC-CO_2 foam at high temperatures and pressures was measured by a capillary tube viscometer (internal diameter = 4 mm and length = 8,000 mm) (**Figure 2**). Foaming agents and SC-CO_2 were coinjected into the capillary tube in a gas-liquid ratio of 2:1. The pressure difference in the capillary tube was recorded as a function of time after SC-CO_2 foam reached the steady-state. The shear rate and the shear stress at

FIGURE 1 | Schematic diagram of the apparatus to evaluate foam stability.
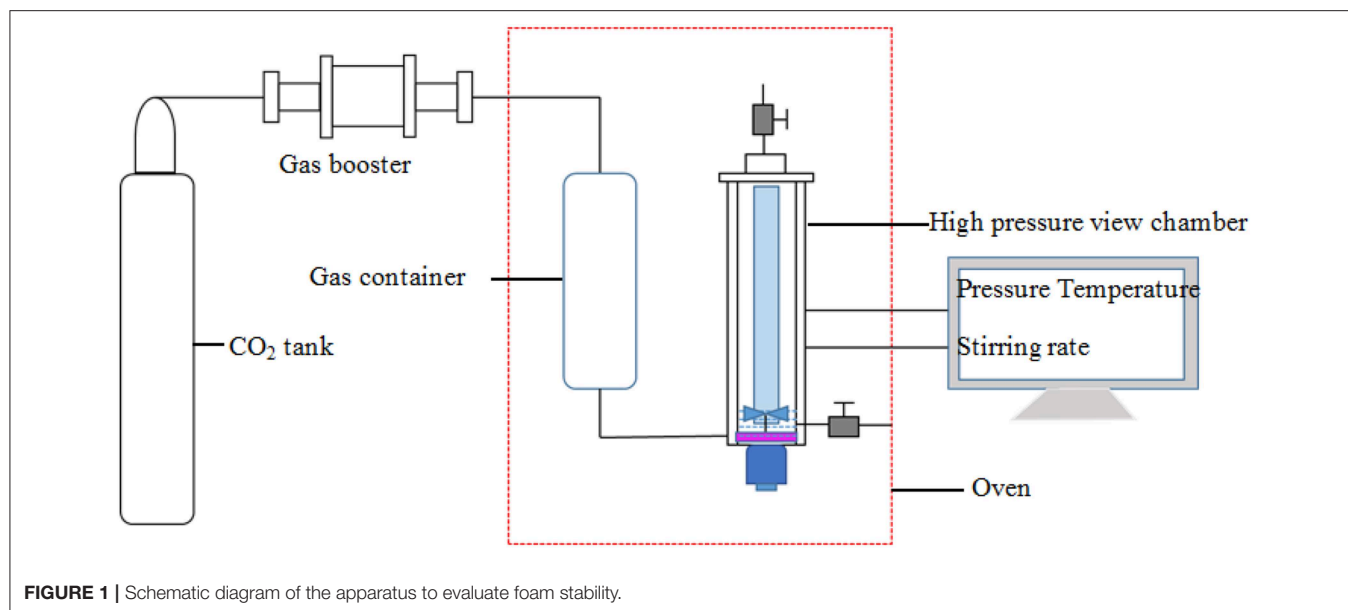
the foam wall were calculated by Equations (1) and (2). As a non-Newtonian fluid, the rheological characteristics of SC-CO_2 foam was described by the power-law model (Equation 3) (Xiao et al., 2017). The power-law exponent and the consistency coefficient were obtained from the logarithm plot of shear stress vs. shear rate. The shear rate and the apparent viscosity at the SC-CO_2 foam wall were calculated by Equations 4 and 5.

$$\gamma_N = \frac{8v_f}{D} \tag{1}$$

$$\tau_N = \frac{D\Delta P}{4L} \tag{2}$$

$$\tau = K\gamma^n \tag{3}$$

$$\gamma = \gamma_N \left(\frac{3n+1}{4n} \right) \tag{4}$$

$$\mu_a = \frac{\tau}{\gamma} = K\gamma^{n-1} \tag{5}$$

where v_f is the velocity of SC-CO_2 foam in the capillary, D is the inner diameter of the capillary tube, ΔP is the pressure difference between two capillary ends, L is the length of the capillary tube, n and k are the power-law exponent and the consistency coefficient, respectively, and μ_a is the apparent viscosity of SC-CO_2 foam.

Steady-State SC-CO_2 Foam Test Under HTHP Conditions

The foaming capacity and the microstructures of SC-CO_2 foam were evaluated by the core flooding experiment, and the schematic diagram of the flow loop apparatus is exhibited in **Figure 2**. The permeability and porosity of the foam were first determined. Foaming agents and CO_2 were coinjected into the core in a gas-liquid ratio of 2:1 until the foam flow reached the steady-state. The steady-state foam was then injected in the high-pressure view cell (path length of 100 μm). The foam flow graphs

were obtained by a Leica S6D camera. The parameters of the cores and foaming agent compositions are presented in **Table 1**. The resistance factor was calculated to characterize the foam strength, and the bubble size was detected by ImageJ software.

The resistance factor was calculated through the following equation:

$$RF = \frac{k_w}{\mu_w} \Big/ \frac{k_f}{\mu_f} = \frac{P_f}{P_0} \tag{6}$$

Where RF is the resistance factor, k_w is the effective permeability of water, μ_w is water viscosity, k_f is the effective permeability of foam, μ_f is foam viscosity, P_f is the pressure difference produced by SC-CO_2 foam, and P_0 is the pressure difference produced by formation water.

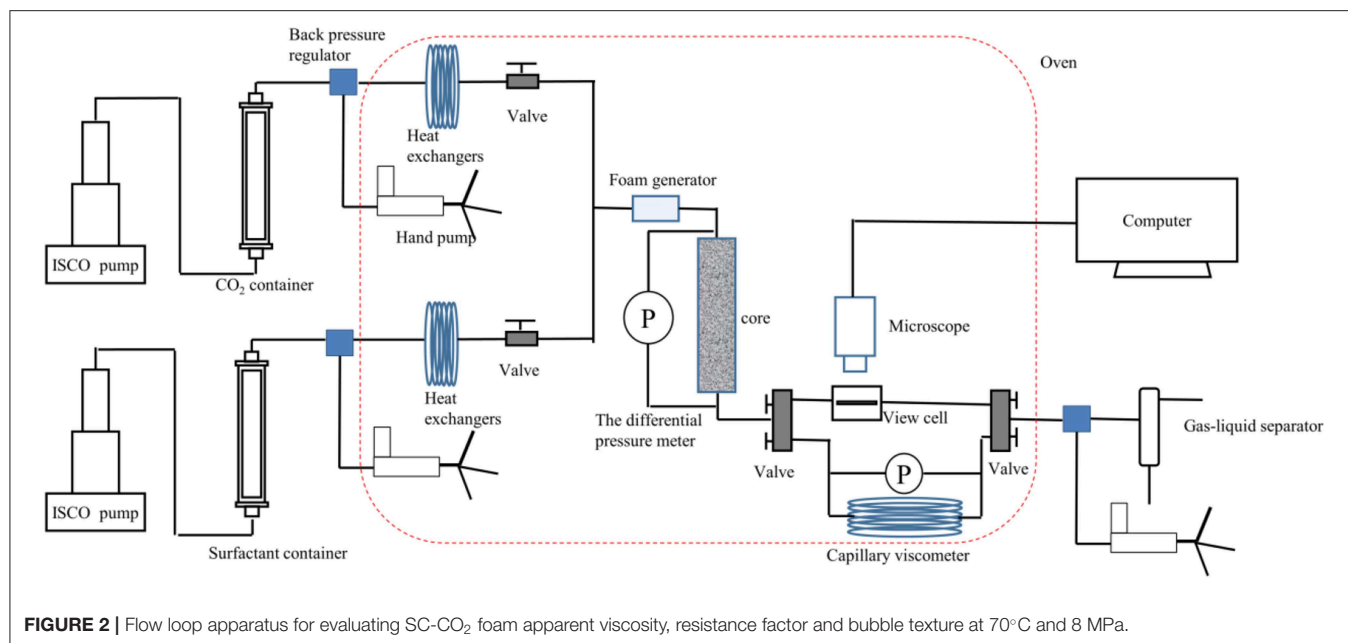## Measurement of Surface Rheological Properties Under HTHP Conditions

The dilational surface elasticity between CO_2 and surfactant solutions were measured by an interfacial tensiometer (Rame-hart instrument, France) based on the oscillating drop method). The surface elasticity (E) of SC-CO_2 foam was calculated as:

$$E = \frac{d\gamma}{d \ln A} \tag{7}$$

The surface dilational viscosity (η_d) of SC-CO_2 foam was determined as:

$$\Delta\gamma = \eta_d \frac{d \ln A}{dt} \tag{8}$$

The surface dilational modulus of SC-CO_2 foam was calculated as:

FIGURE 2 | Flow loop apparatus for evaluating SC-CO_2 foam apparent viscosity, resistance factor and bubble texture at 70°C and 8 MPa.

TABLE 1 | Summary of core flooding tests.

Run no.	Length/cm	Cross-sectional area/cm^2	Pore volume/cm^2	Permeability/mD	Chemical formula
1	9.95	4.79	10.21	657.7	0.05% HHSB
2	9.90	4.79	10.34	654.5	0.05% HHSB + 0.3% NPs
3	9.78	4.79	10.34	646.8	0.05% HHSB + 0.5% NPs
4	9.51	4.79	9.9	628.6	0.05% HHSB + 0.7% NPs

$$E^* = E' + iE'' \tag{9}$$

where γ denotes surface tension, A is the surface area of SC-CO_2 foam, $\Delta\gamma$ is the surface tension difference between a constantly (logarithmically) expanding surface and the equilibrium surface, E' is the storage modulus, and E'' is the loss modulus.

RESULTS AND DISCUSSION

Effects of Silica NPs on the Foaming Capacity of SC-CO_2 Foam

When SC-CO_2 foam was formed in the HPHT cell under the mixing of CO_2 and foaming agents, the stability of SC-CO_2 foam was mainly controlled by the gravitational drainage of lamellae, thus resulting in film thinning and the rupture of foam bubbles (Heller and Kuntamukkula, 1987). The drainage rate was used to characterize the stability of SC-CO_2 foam. The evolution of drainage volume with time is displayed in **Figure 3**. The drainage rate of SC-CO_2 foam without NPs was very fast, and the drainage volume reached 60 mL in less than a min. However, the drainage rate declined rapidly after the addition of NPs. It was also noticed that when the drainage liquid volume was <50 mL, a relatively fast drainage rate was achieved. However, when the drainage liquid volume was >50 mL, the drainage rate became very slow. **Table 2** summarized the change of drainage rare as a function

of nanoparticle concentration. The drainage rate decreased by a factor of about 50 after 50 mL of liquid was separated from SC-CO_2 foam, and this phenomenon reveals that the adsorption of NPs on bubble lamellae occurred very slowly. In the initial stage of the foam formation, NPs mainly remained in the liquid phase and the drainage rate was very high, thus generating an unstable foam film (**Figure 4A**). With the prolonged aging time, NPs tended to rest at the liquid-gas interface (**Figure 4B**). In addition, the solution color of foaming agents was gray before the foaming test (**Figure 5A**). However, after the foaming test (**Figure 5B**), the solution color became nearly clear (**Figure 5C**), which indicated that NPs were adsorbed at the liquid-gas interface rather than in the aqueous phase. The adsorption of NPs at the gas-liquid interface has an effect on the disjoining pressure, which includes electrostatic, steric, and structural interactions (Exerowa et al., 1987). As the film thickness decreased further due to the film drainage by gravity, the disjoining pressure increased to a maximum at a critical film thickness. If the van der Waals interactions exceeded the electrostatic repulsion, the disjoining pressure would decline sharply (**Figure 4A**). Hence, the film became very unstable and large drainage rate was obtained. However, with continuous adsorption of NPs at the gas-liquid interface, a large repulsive steric forces was induced, which could raise the disjoining pressure (**Figure 4B**). With the increase in disjoining pressure, foam became stable and a slow drainage rate was attained (Dhanuka et al., 2006).
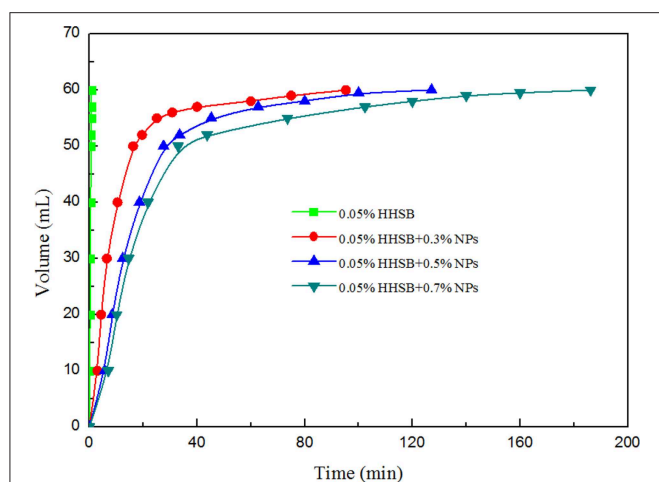
FIGURE 3 | Change in the drainage volume as a function of time at 70°C and 8 MPa for different nanoparticle concentration at the HHSB concentration of 0.05%.

TABLE 2 | The initial foaming volume and drainage rate as a function of nanoparticle concentration.

Foaming agents	Initial foaming volume/mL	V$_{drainage}$ < 50 mL	V$_{drainage}$ > 50 mL
		Drainage rate (mL/min)	Drainage rate (mL/min)
0.05% HHSB	570	81.08	52
0.05% HHSB + 0.3% NPs	545	2.84	0.055
0.05% HHSB + 0.5% NPs	535	1.76	0.048
0.05% HHSB + 0.7% NPs	520	1.48	0.029

Effect of Salinities and Temperature on SC-CO$_2$ Foam

When CO$_2$ foam is applied for mobility control in oil fields, temperature and salinity manifest great effects on foam capacity and stability. Therefore, in order to investigate the effects of salinity and temperature on the SC-CO$_2$ foam stabilized by NPs, the half-life of the foam was used to characterize its stability. **Figure 6** depicts the effects of salinity on the foaming volume and the half-life of SC-CO$_2$ foam. It is noticeable that with an increase in salinity, the foaming volume decreased slightly and the half-life of the foam increased greatly. This is attributed to the continuous adsorption of NPs on the gas-liquid interface. The dynamic light scattering test revealed that the mean zeta potential of NPs was about −22.63 mV. In the presence of salt ions, negative charges at nanoparticles surface were screened and the electrostatic repulsion between NPs became weak, thus accumulating more NPs on the gas-liquid interface to enhance the stability of SC-CO$_2$ foam (Basheva et al., 1999; Adamczyk, 2003; Gupta and Basu, 2005). **Figure 7** illustrates the changes in foaming volume and half-life of SC-CO$_2$ foam at different temperatures. It is evident that with the increasing temperature, the drainage rate increased

rapidly, thus resulting in the destabilization of SC-CO$_2$ foam. Although increasing temperature made nanoparticle stability decline and facilitated the adsorption of nanoparticles at gas-liquid interface, the gas transfer rate across the film was accelerated at high temperatures, thereby causing film thinning and bubble rupture.

Apparent Viscosity of SC-CO$_2$ Foam

The power-law model was adopted to describe the non-Newtonian behavior of SC-CO$_2$ foam. The logarithmic curves of shear stress vs. shear rate and the corresponding fitted curves are displayed in **Figure 8**. **Table 3** depicts the necessary parameters and equations of the power-law model. Slopes less than unity indicates pseudoplastic fluids, whereas slopes greater than unity imply dilatant fluids. Based on the power-law model, the apparent viscosity of SC-CO$_2$ foam was calculated as a function of shear rate. **Figure 9** presents the apparent viscosity of the NPs-stabilized SC-CO$_2$ foam at 70°C and 8 MPa. It is discernible that SC-CO$_2$ foam behaved in shear-thinning or a pseudo-plastic manner and its apparent viscosity started to decline with the increasing shear rate. It is evident that NP concentration significantly affected the rheological behaviors of SC-CO$_2$ foam. SC-CO$_2$ foam without NPs had a flow behavior index n of 0.61, whereas the flow behavior index decreased to 0.2~0.4 for the NPs-stabilized CO$_2$ foam. Furthermore, SC-CO$_2$ foam without NPs exhibited relatively low apparent viscosity (the values were <20 mPa·s at different shear rates). With an increase in NP concentration, the apparent viscosity of SC-CO$_2$ foam increased greatly. When NP concentration was 0.7%, the apparent viscosity reached 80 mPa·s at a shear rate of 26 s^{-1}. It happened because the apparent viscosity of SC-CO$_2$ foam was controlled by the foam structure and lamella properties (Bonilla and Shah, 2000). SC-CO$_2$ foam was generated by coinjecting foaming agents and SC-CO$_2$ through 50 μm pores of the foam generator and then flowing through the capillary tube. The initial bubble size was the same for SC-CO$_2$ foams stabilized by different foam agents. However, the foam structure started to coarsen as foam flowed in the capillary tube due to gas transfer and capillary pressure. At the same shear rate, more NP adsorption at the liquid-gas interface would provide thick protective shells around the bubbles against foam coarsening and gas transfer, thereby resulting in dense texture and higher apparent viscosity (Alargova et al., 2004; Stephanie et al., 2008).

Evaluation of Resistance Factor During the Core Flooding Experiment

Resistance factor is used to characterize the strength of the SC-CO$_2$ foam. A large resistance factor means lower foam mobility, which depends considerably on foam texture. The effects of NP concentration on resistance factor are presented in **Figure 10**. It is noticeable that the value of the resistance factor gradually increased with the increasing NP concentration. It could be deduced that the NPs-stabilized SC-CO$_2$ foam had much finer foam texture and denser bubble distribution. The gravitational drainage of liquid through foam lamellae was not the main mechanism of foam rupture in the porous medium. When the
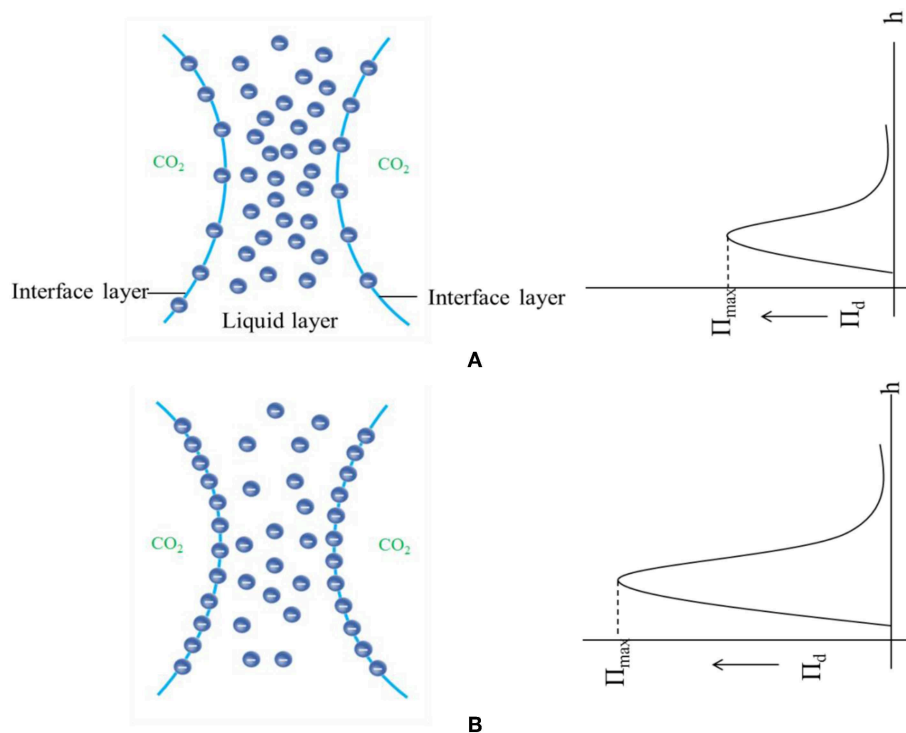
FIGURE 4 | Schematic of disjoining pressure between foam films as a function of film thickness before **(A)** and after **(B)** nanoparticle adsorption at the gas-liquid interface.
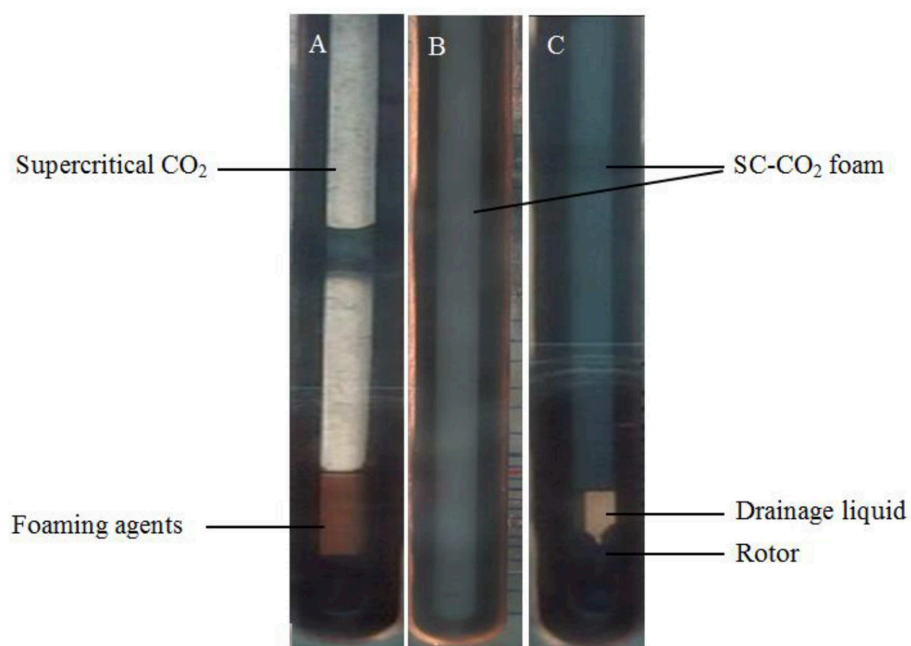

FIGURE 5 | The Foaming process of SC-CO_2 foams stabilized with 0.05% HHSB and 0.5% NPs at 8 MPa and 70°C. **(A)** The foaming agents before shearing, **(B)** SC-CO_2 foam immediately after shearing was stopped, and **(C)** the drainage process after shearing was stopped.
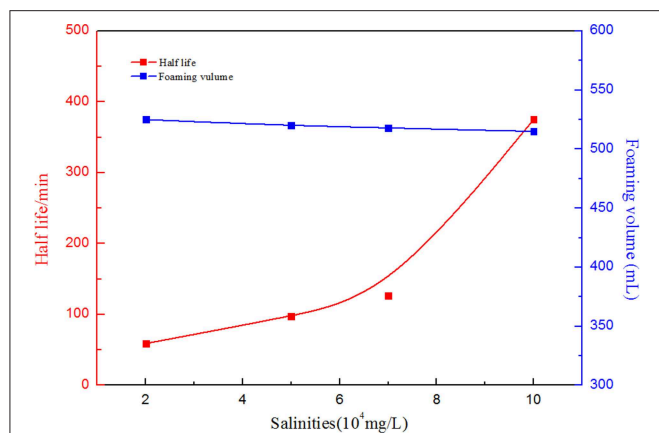
FIGURE 6 | Foaming volume and half-life as a function of salinities at 70°C and 8 MPa. for SC-CO_2 foam stabilized by 0.05% HHSB and 0.5% NPs.
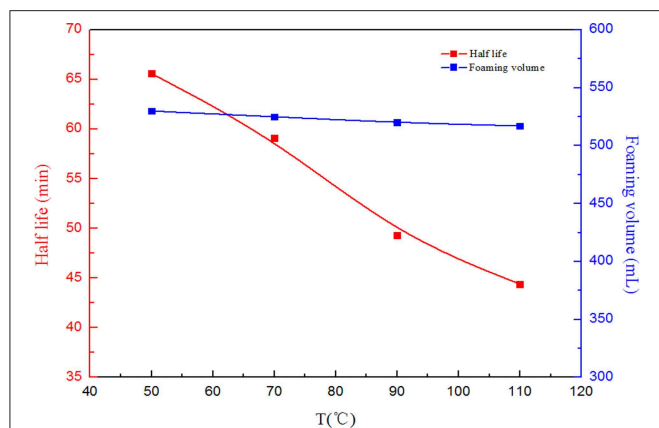

FIGURE 7 | Foaming volume and half-life as a function of temperature at pressure of 8 MPa for SC-CO_2 foam stabilized by 0.05% HHSB and 0.5% NPs.
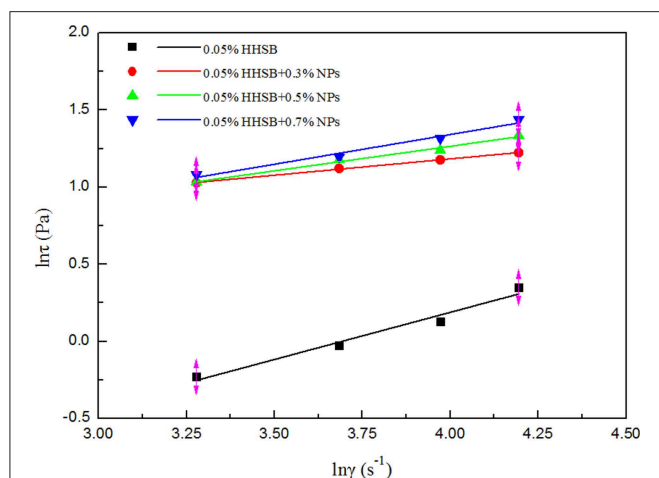

FIGURE 8 | Fit curves between shear rate and apparent wall shear stress for SC-CO_2 foams with different nanoparticles.

TABLE 3 | The parameters of power-law equations for the SC-CO_2 foam with different NPs.

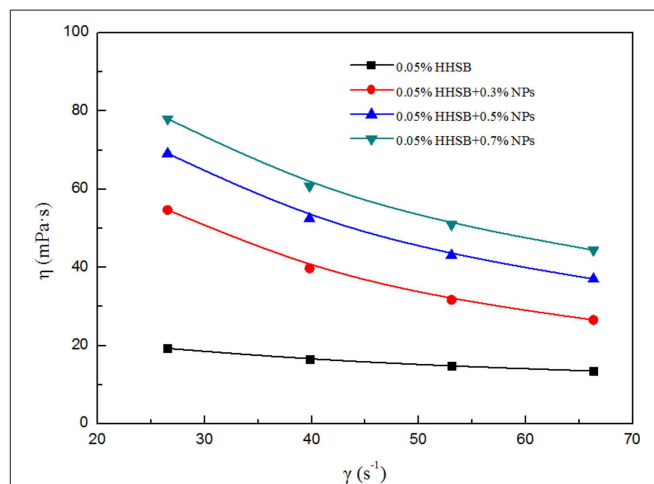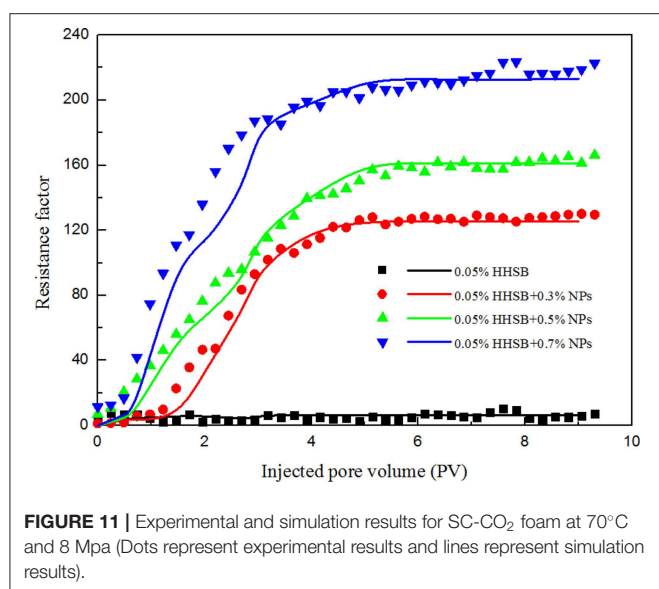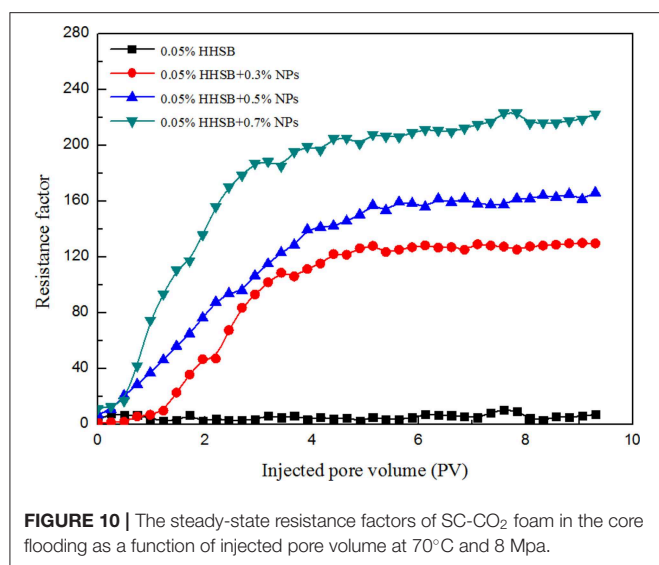| Nanoparticle concentration/%	n	K'	K	Equation
0	0.61	0.080	0.073	$\tau = 0.073\gamma^{-0.39}$
0.3	0.21	1.40	1.22	$\tau = 1.22\gamma^{-0.79}$
0.5	0.32	0.99	0.86	$\tau = 0.86\gamma^{-0.68}$
0.7	0.39	0.82	0.72	$\tau = 0.72\gamma^{-0.61}$

FIGURE 9 | Apparent viscosity of SC-CO_2 foam as a function of shear rate with different nanoparticles at 70°C and 8 MPa.

foam flowed through the porous medium, the main mechanisms of foam rupture were lamellae collapse due to capillary pressure and gas diffusion across foam lamellae. It can be inferred that NPs significantly enhanced the stability of SC-CO_2 foam in the porous media by reducing bubble coalescence rates. In order to explore the mechanisms of increased resistance factor in the presence of NPs in the porous media, the stochastic population balance (SPB) model was employed to describe the flow behavior of the NPs-stabilized SC-CO_2 foam (Zitha and Du, 2010; Du et al., 2011). In the SBP model, the bubble generation in the porous media was regarded as a macroscopic stochastic process. The net foam generation (q_f) was obtained by Equation (9).

$$q_f = \varphi S_f K_g (n_\infty - n) \qquad (10)$$

where φ is the porosity of the core, S_f denotes foam saturation, K_g is the foam generation rate, n_∞ is the maximum bubble density, and n signifies bubble density.

With involving two parameters of foam generation rate K_g and maximum bubble density n_∞, the SBP model shows considerable conveniences to characterize the strength of NPs-stabilized SC-CO_2 foam. Bubble density was controlled by bubble generation and coalescence mechanisms: capillary snap-off, lamella division and leave behind generated foams and
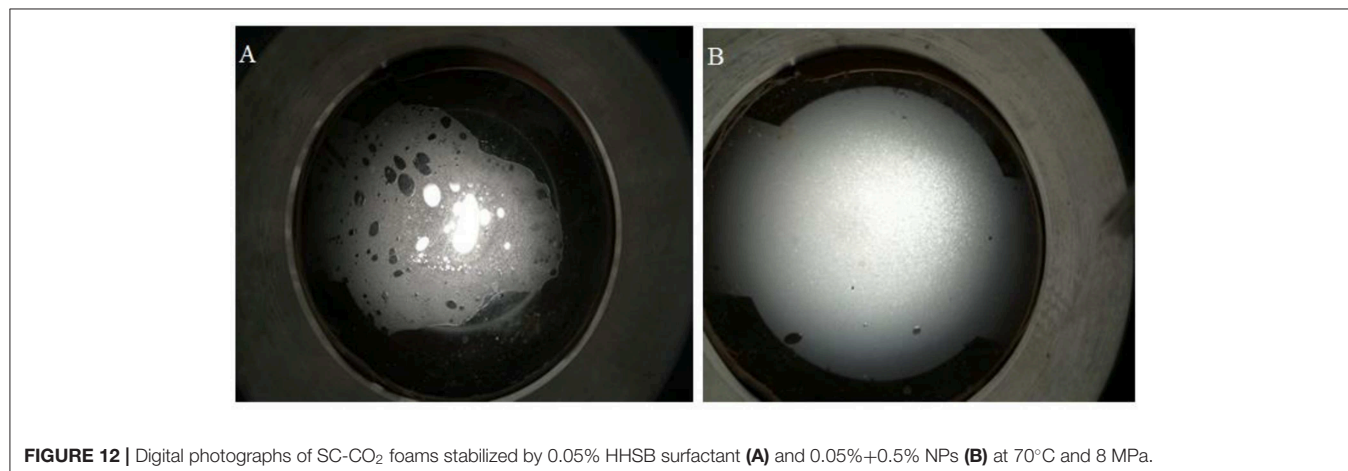
FIGURE 10 | The steady-state resistance factors of SC-CO_2 foam in the core flooding as a function of injected pore volume at 70°C and 8 Mpa.

FIGURE 11 | Experimental and simulation results for SC-CO_2 foam at 70°C and 8 Mpa (Dots represent experimental results and lines represent simulation results).

increased the bubble density, whereas gas transfer and capillary suction destroyed foams and diminished the bubble density. With addition of nanoparticles, the gas transfer rate between bubbles was decreased and the ability to withstand capillary pressure was improved in porous media, thereby resulting in larger maximum bubble density and higher generation rate. The control equations of the two-phase flow process in the one-dimensional domain were solved by the IMPES algorithm. The simulation parameters of the SBP model are presented in **Tables S1–S4**. **Figure 11** illustrates the obtained experimental and simulation results for the SPB model, and it is showed that simulation and experimental results were in good agreement for the resistance factor.

Microstructures of SC-CO_2 Foam

The microstructure of SC-CO_2 foam from the exit of the core was observed by the microscope. **Figure 12** displays the digital photographs of SC-CO_2 foams with and without NPs immediately after foam flow was stopped. SC-CO_2 foam with NPs had a more compact bubble structure, which blocked nearly all the light below the optical cell. In order to distinguish SC-CO_2 foam texture, **Figure 13** displays the microscope images of SC-CO_2 foams as a function of time. The mean bubble size was about 20~30 μm after the foam flowed into the high-pressure cell for 10 min. Since the space between sapphire windows was about 100 μm, multiple bubble layers existed in the cell. With the prolonged experiment, the mean bubble size increased for SC-CO_2 foams with and without NPs. However, the increase rate of NPs-stabilized SC-CO_2 foams was lower than that of the foams without NPs. After executing aging for 1 h, the mean bubble size of NPs-stabilized SC-CO_2 foams increased to 40~50 μm, whereas the mean bubble size of the foams without NPs reached 70~80 μm. It can be concluded that coalescence rate of SC-CO_2 foam became slower with increasing nanoparticle concentration.

Surface Elasticity of SC-CO_2 Foam

The foam stability was related to the surface interfacial rheological properties of the bubble film. A large dilatational surface elasticity could dampen external film fluctuations induced by temperature, pressure, or salinity (Heller and
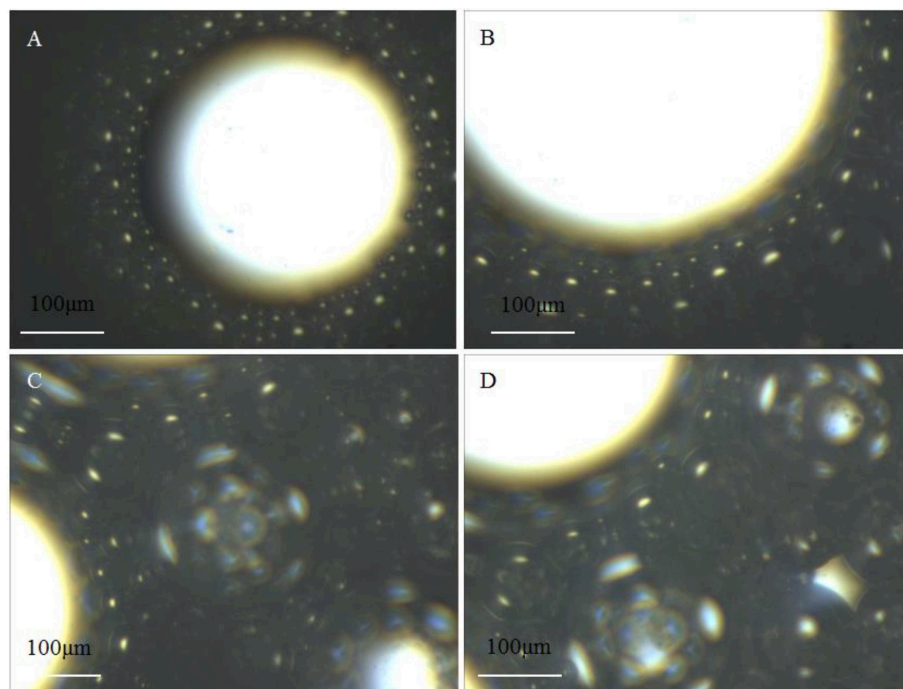

FIGURE 12 | Digital photographs of SC-CO_2 foams stabilized by 0.05% HHSB surfactant **(A)** and 0.05%+0.5% NPs **(B)** at 70°C and 8 MPa.

FIGURE 13 | Micrographas of SC-CO$_2$ foams stabilized with 0.05 and 0.5% NPs HHSB at 70°C and 8 MPa aging for 10 min **(A)**, 40 min **(B)**, 70 min **(C)**, and 100 min **(D)**.
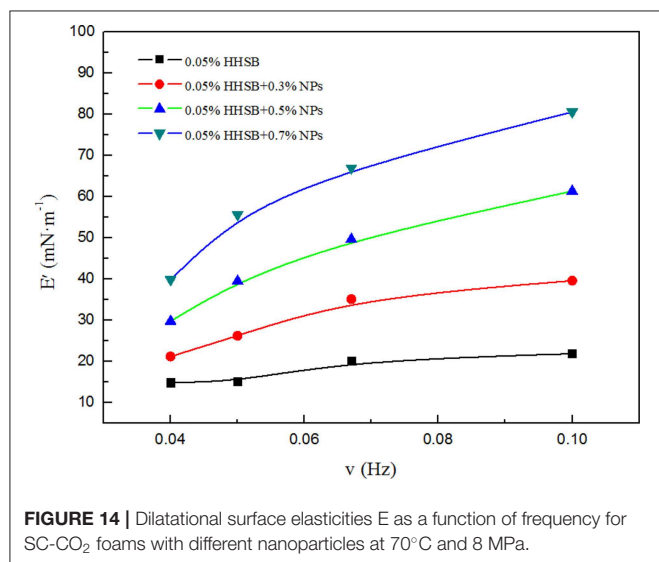

FIGURE 14 | Dilatational surface elasticities E as a function of frequency for SC-CO$_2$ foams with different nanoparticles at 70°C and 8 MPa.
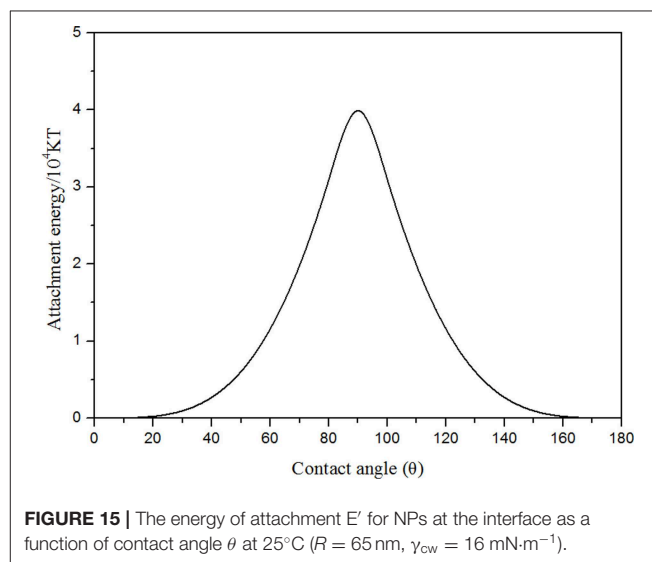

FIGURE 15 | The energy of attachment E' for NPs at the interface as a function of contact angle θ at 25°C ($R = 65$ nm, $\gamma_{cw} = 16$ mN·m^{-1}).

Kuntamukkula, 1987; Basheva et al., 1999; Adkins et al., 2010). In order to explore the mechanisms of foam stabilization, the dilatational surface elasticity between CO$_2$ and foam agents were measured as a function of frequency at 70°C and 8 MPa. It is noticeable that the dilatational surface elasticity was increased with increasing NP concentration (**Figure 14**). When NP concentration reached 0.7%, the dilatational surface elasticity could reach up to 4 times as large as that of surfactant solutions

without NPs. Surfactant adsorption was a dynamic process where adsorption and desorption are present simultaneously, and surfactant molecules adsorbed at the CO$_2$-water interface easily underwent desorption from the interface due to external disturbance (Li et al., 2017). In comparison to HHSB molecules, NPs were adsorbed more strongly at the CO$_2$-water interface, thus it was difficult for them to be desorbed from the interface. The energy of attachment (E), which is required to remove NPs

from the solid-liquid interface, can be expressed as (Stephanie et al., 2008).

$$E = \pi R^2 \gamma_{CW}(1 \pm \cos\theta)^2 \qquad (11)$$

where r is the particle radius, γ_{CW} is the interfacial tension between SC-CO$_2$ and water, θ is the contact angle particles make with the water phase.

For hydrophilic NPs ($0° < \theta < 90°$ and $\cos\theta > 0$), the sign in the bracket would be negative. For hydrophobic NPs ($90° < \theta < 180°$ and $\cos\theta < 0$), the sign in the bracket would be positive. Based on the above equation, the energy of attachment was calculated as a function of θ, and the corresponding results are displayed in **Figure 15**. It is noticeable that NPs were most strongly adsorbed at the interface for $85° < \theta < 95°$. The hydrophilic nanoparticles were dispersed in water phase and it can be inferred that the contact angle particles make with the water phase is lower than 90°. If the contact angle was >20°, the energy of attachment was large on the order of magnitude of 10^4 KT. Therefore, when the bubble film confronted external disturbances (temperature and capillary pressure), NPs were strongly adsorbed at the CO$_2$-water interface due to the large energy of attachment. NPs adsorbed at the CO$_2$-water interface could result in higher dilatational surface elasticity, which dampened external disturbances and resisted the deformation of foam lamellae (Basheva et al., 1999; Stubenrauch and Miller, 2004).

CONCLUSIONS

A novel foaming agent composed of zwitterionic surfactant and silica nanoparticles was developed to stabilize SC-CO$_2$ foam. The foaming ability and stability of SC-CO$_2$ foam was investigated at 70°C and 8 MPa. The drainage rate of the SC-CO$_2$ foam first was fast and then started to decelerate with the increase in NP adsorption at the gas-liquid interface. NP adsorption at the interface could enhance the disjoining pressure, thereby preventing film thinning. The stability of SC-CO$_2$ foam got improved with the increase in salinity due to the screened electrostatic repulsion between negatively-charged silica NPs. NP-stabilized SC-CO$_2$ foam showed power-law shear thinning rheological behavior and the apparent viscosity increased up to 80 mPa·s with increasing nanoparticle. The texture of SC-CO$_2$ foam was observed during steady-state foam flow, and the average effluent bubble size was found as 10~20 μm. The coalescence rate of SC-CO$_2$ foam gradually became very slow with the increasing NP concentration. Based on the SBP model, the resistance factor of SC-CO$_2$ foam was simulated as a function of NP concentration by considering its generation rate and maximum bubble density. The resistance factor obtained from the SBP model agreed well with experimental results. Oscillation measurements proved the improvement of SC-CO$_2$ foam stability with the increasing NP concentration was attributed to an increase in surface elasticity.

DATA AVAILABILITY STATEMENT

The datasets generated for this study are available on request to the corresponding author.

AUTHOR CONTRIBUTIONS

WL participated in the design of the manuscript and drafted the manuscript. FW, CX, and JO came up with ideas for the manuscript. LS analyzed experimental results. MD carried out experiments. DD and PL revised the manuscript.

FUNDING

SUPPLEMENTARY MATERIAL

The Supplementary Material for this article can be found online at: https://www.frontiersin.org/articles/10.3389/fchem.2019.00718/full#supplementary-material

REFERENCES

Adamczyk, Z. (2003). Particle adsorption and deposition: role of electrostatic interactions. *Adv. Colloid Interface Sci.* 100–102, 267–347. doi: 10.1016/S0001-8686(02)00062-3

Adkins, S. S., Chen, X., Chan, I., Torino, E., Nguyen, Q. P., Sanders, A. W., et al. (2010). Morphology and stability of CO2-in-water foams with nonionic hydrocarbon surfactants. *Langmuir* 26, 5335–5348. doi: 10.1021/la903663v

Alargova, R. G., Warhadpande, D. S., Paunov, V. N., and Velev, O. D. (2004). Foam superstabilization by polymer microrods. *Langmuir* 20, 10371–10374. doi: 10.1021/la048647a

Alzobaidi, S., Lotfollahi, M., Kim, I., Johnston, K., and Dicarlo, D. (2017). Carbon dioxide-in-brine foams at high temperatures and extreme salinities stabilized with silica nanoparticles. *Energy Fuels* 31, 10680–10690. doi: 10.1021/acs.energyfuels.7b01814

Aveyard, R. H., and Clint, J. (1995). Liquid droplets and solid particles at surfactant solution interfaces. *J. Chem. Soc. Faraday Trans.* 91:2681. doi: 10.1039/ft9959102681

Ayesh, A., Salazar, R. O., Farajzadeh, S., Vincent-Bonnieu, S., and Rossen, W. R. (2017). Foam diversion in heterogeneous reservoirs: effect of permeability and injection method. *SPE J.* 22, 1402–1415. doi: 10.2118/179650-PA

Basheva, E. S., Ganchev, D. N., Denkov, N., Kasuga, K., Satoh, N., and Tsujii, K. (1999). Role of betaine as foam booster in the presence of silicone oil drops. *Langmuir* 16, 1000–1013. doi: 10.1021/la990777+

Bonilla, L. F., and Shah, S. N. (2000). "Experimental investigation on the rheology of foams," in *Paper Presented at the SPE/CERI Gas Technology Symposium* (Calgary, AB). doi: 10.2118/59752-MS

Chang, D., Alzobaidi, S., Jian, G., Zhang, L., Biswal, S. L., Hirasaki, G. J., et al. (2018). Carbon dioxide/water foams stabilized with a zwitterionic surfactant

at temperatures up to 150 °C in high salinity brine. *J. Petrol. Sci. Eng.* 166, 880–890. doi: 10.1016/j.petrol.2018.03.071

Chang, S.-H., and Grigg, R. B. (1999). Effects of foam quality and flow rate on CO₂-foam behavior at reservoir temperature and pressure. *SPE Reservoir Eval. Eng.* 2, 248–254. doi: 10.2118/56856-PA

Chen, Y., Elhag, A. S., Cui, L., Worthen, A. J., Reddy, P. P., Noguera, J. A., et al. (2015). CO₂-in-water foam at elevated temperature and salinity stabilized with a nonionic surfactant with a high degree of ethoxylation. *Ind. Eng. Chem. Res.* 54, 4252–4263. doi: 10.1021/ie503674m

Da, C., Jian, G., Alzobaidi, S., Yang, J., Biswal, S. L., Hirasaki, G. J., et al. (2018). Design of CO₂-in-water foam stabilized with switchable amine surfactants at high temperature in high-salinity brine and effect of oil. *Energy Fuels* 32, 12259–12267. doi: 10.1021/acs.energyfuels.8b02959

Dhanuka, V. V., Dickson, J. L., Ryoo, W., and Johnston, K. (2006). High internal phase CO₂-in-water emulsions stabilized with a branched nonionic hydrocarbon surfactant. *J. Colloid Interface Sci.* 298, 406–418. doi: 10.1016/j.jcis.2005.11.057

Du, D. X., Zitha, P. L. J., and Vermolen, F. J. (2011). Numerical analysis of foam motion in porous media using a new stochastic bubble population model. *Transp. Porous Media* 86, 461–474. doi: 10.1007/s11242-010-9631-7

Exerowa, D., Kolarov, T., and Khristov, K. (1987). Direct measurement of disjoining pressure in black foam films. I. Films from an ionic surfactant. *Colloids Surfaces* 22, 161–169. doi: 10.1016/0166-6622(87)80218-4

Farajzadeh, R., Andrianov, A., Krastev, R., Hirasaki, G. J., and Rossen, W. R. (2012). Foam–oil interaction in porous media: implications for foam assisted enhanced oil recovery. *Adv. Colloid Interface Sci.* 183–184, 1–13. doi: 10.2118/154197-MS

Gupta, J. K., and Basu, S. (2005). Simultaneous aggregation and sedimentation of silica particles in the presence of surfactants. *Colloids Surfaces A Physicochem. Eng. Aspects* 255, 139–143. doi: 10.1016/j.colsurfa.2004.12.010

Heller, J. P., and Kuntamukkula, M. S. (1987). Critical review of the foam rheology literature. *Ind. Eng. Chem. Res.* 26, 318–325. doi: 10.1021/ie00062a023

Horozov, T. S. (2008). Foams and foam films stabilised by solid particles. *Curr. Opin. Colloid Interface Sci.* 13, 134–140. doi: 10.1016/j.cocis.2007.11.009

Kalyanaraman, N., Arnold, C., Gupta, A., Tsau, J., and Barati, R. (2016). Stability improvement of CO₂ foam for enhanced oil-recovery applications using polyelectrolytes and polyelectrolyte complex nanoparticles. *J. Appl. Polym. Sci.* 134:44491. doi: 10.2118/174650-MS

Li, W., Dai, C., Ouyang, J., Aziz, H., Jiaping, T., He, X., et al. (2017). Adsorption and retention behaviors of heterogeneous combination flooding system composed of dispersed particle gel and surfactant. *Colloids Surfaces A Physicochem. Eng. Aspects* 538, 250–261. doi: 10.1016/j.colsurfa.2017.11.008

Lotfollahi, M., Farajzadeh, R., Delshad, M., Varavei, A. R., and Rossen, W. (2016). Comparison of implicit-texture and population-balance foam models. *J. Nat. Gas Sci. Eng.* 31, 184–197. doi: 10.1016/j.jngse.2016.03.018

Mukherjee, J., Norris, S. O., Nguyen, Q. P., Scherlin, J. M., Vanderwal, P. G., and Abbas, S. (2014). "CO₂ foam pilot in Salt Creek Field, Natrona County,

WY: Phase I: laboratory work, reservoir simulation, and initial design," in *Paper Presented at the SPE Improved Oil Recovery Symposium* (Tulsa, OK). doi: 10.2118/169166-MS

Petkova, R., Tcholakova, S., and Denkov, N. (2012). Foaming and foam stability for mixed polymer-surfactant solutions: effects of surfactant type and polymer charge. *Langmuir* 28, 4996–5009. doi: 10.1021/la3003096

Sanders, A. W., Jones, R. M., Linroth, M. A., and Nguyen, Q. P. (2012). "Implementation of a CO₂ foam pilot study in the SACROC field: performance evaluation," *Paper Presented at the SPE Annual Technical Conference and Exhibition* (San Antonio, TX). doi: 10.2118/160016-MS

Stephanie, S. A., Dhiren, G., Jasper, L. D., Stephen, E. W., and Keith, J. (2008). Water-in-carbon dioxide emulsions stabilized with hydrophobic silica particles. *Phys. Chem. Chem. Phys.* 9, 6333–6343. doi: 10.1039/b711195a

Stubenrauch, C., and Miller, R. (2004). Stability of foam films and surface rheology: an oscillating bubble study at low frequencies. *J. Phys. Chem. B* 108, 6412–6421. doi: 10.1021/jp049694e

Tamura, T., Kaneko, Y., and Nikaido, M. (1997). Stability factors of foam film in contrast to fluctuation induced by humidity reduction. *J. Colloid Interface Sci.* 190, 61–70. doi: 10.1006/jcis.1997.4819

Worthen, A. J., Parikh, P. S., Chen, Y., Bryant, S. L., Huh, C., and Johnston, K. P. (2014). Carbon dioxide-in-water foams stabilized with a mixture of nanoparticles and surfactant for CO₂ storage and utilization applications. *Energy Procedia* 63, 7929–7938. doi: 10.1016/j.egypro.2014.11.827

Xiao, C., Balasubramanian, S. N., and Clapp, L. W. (2017). Rheology of viscous CO₂ foams stabilized by nanoparticles under high pressure. *Ind. Eng. Chem. Res.* 56, 8340–8348. doi: 10.1021/acs.iecr.7b01404

Zhang, G., and Seright, R. S. (2007). "Conformance and mobility control: foams versus polymers," *Paper Presented at the International Symposium on Oilfield Chemistry* (Houston, TX). doi: 10.2118/105907-MS

Zhang, Y., Gao, M. W., You, Q., Fan, H. F., Li, W. H., Liu, Y. F., et al. (2019). Smart mobility control agent for enhanced oil recovery during CO2 flooding in ultra-low permeability reservoirs. *Fuel* 241, 442–450. doi: 10.1016/j.fuel.2018.12.069

Zitha, P. L. J., and Du, D. X. (2010). A new stochastic bubble population model for foam flow in porous media. *Transport Porous Media* 83, 603–621. doi: 10.1007/s11242-009-9462-6